GEOPHYSICS, VOL. 85, NO. 2 (MARCH-APRIL 2020); P. JM1–JM11, 14 FIGS.
10.1190/GEO2018-0779.1

Apsu — A new compact surface nuclear magnetic resonance system for groundwater investigation

Jakob Juul Larsen[1], Lichao Liu[2], Denys Grombacher[2], Gordon Osterman[1], and Esben Auken[2]

ABSTRACT

Surface nuclear magnetic resonance (NMR) is emerging as a competitive method for aquifer exploration due to its direct sensitivity to subsurface water, but the method still has several shortcomings, for example, a signal-to-noise ratio that is often poor, long survey times, and bulky equipment. We have developed Apsu, a new surface NMR system designed for near-surface groundwater investigations. It provides several features such as a compact transmitter unit, separated, small receiver coils, wireless connections between multiple receivers, quasi-zero dead time, and robust phase determination. The transmitter unit is powered by a lightweight generator, and it drives a triangular current in an untuned 50×50 m transmitter coil. The peak current of the triangular waveform is up to 145 A, with an effective peak current of 105 A at a Larmor frequency of 2 kHz, corresponding to a 30 m depth of investigation. The frequency and amplitude in each half-oscillation of the transmit pulses can be modulated independently, which gives great flexibility in the pulse design. The receiver uses low-noise preamplifiers and multiple receivers linked to a central unit through Wi-Fi. The use of small receiver coils and wireless connections to multichannel receivers greatly improves the layout configuration flexibility and survey efficiency. The performance of the system under field conditions is demonstrated with high-quality data collected near Silkeborg, Denmark, using on-resonance and numerically optimized modulation pulses.

INTRODUCTION

Surface nuclear magnetic resonance (NMR) is a promising method for groundwater investigations due to its direct sensitivity to hydrogeophysical parameters of interest, such as water content, pore size, and permeability (e.g., Roy and Lubczynski, 2003; Grunewald and Knight, 2011; Behroozmand et al., 2015). To obtain an NMR signal from subsurface groundwater, a surface NMR system needs to generate an oscillating magnetic field to stimulate the nuclear spins of the hydrogen atoms in water molecules out of their equilibrium. To accomplish this, a pulsed oscillating current of up to several hundreds of amperes is injected into a surface transmitter coil. After the pulse is shut off, the nuclear spins continue to precess in the earth's magnetic field while they relax back to equilibrium, which emits an oscillating, exponentially decaying signal. This signal can be recorded by a receiver coil at the surface (e.g., Weichman et al., 2000; Hertrich, 2008). The magnitude of the received NMR signal is only on the order of nV, which makes it challenging to obtain reliable measurements in the presence of natural and anthropogenic noise.

The first generation of surface NMR instruments, HYDROSCOPE and later NUMIS, were single-channel systems that used the same coil for transmitting and receiving signals (Schirov et al., 1991; Bernard, 2007). In this design, an electromechanical relay was used to switch the coil from the transmit to the receive mode. The coil was tuned to the local proton-precession frequency, or the Larmor frequency, in the transmit and receive modes to maximize the excitation current and mitigate noise, respectively. The tuned coil had a high-quality factor Q, which led to slow dissipation of the current after the pulse is terminated if the coil remained in a high Q state. Additionally, the narrow-band acquisition circuit distorted the early-time signal due to the transient response of the filters. Overall, the NUMIS system had a dead time of approximately 20–40 ms, which prevented the measurement of groundwater in the vadose zone, silt-and clay-rich aquifers, and formations with magnetic minerals (Bernard, 2007; Walsh et al., 2011). The first NUMIS

Manuscript received by the Editor 14 November 2018; revised manuscript received 5 November 2019; published ahead of production 10 December 2019; published online 12 February 2020.
[1]Aarhus University, Department of Engineering, Finlandsgade 22, 8200 Aarhus N, Denmark. E-mail: jjl@eng.au.dk; gko@eng.au.dk.
[2]Aarhus University, Hydrogeophysics Group, Department of Geoscience, C. F. Møllers Allé 4, 8000 Aarhus C, Denmark. E-mail: lichao@geo.au.dk (corresponding author); denys.grombacher@geo.au.dk; esben.auken@geo.au.dk.

instruments recorded the NMR envelope directly using an internal synchronous detector, which limits postprocessing flexibility (Legchenko et al., 2002). Due to its susceptibility to ambient electromagnetic noise and its incompatibility with more recent noise-reduction strategies, surface NMR investigation with these types of single-channel instruments was generally restricted to low-noise environments.

A significant improvement of surface NMR occurred with the development of multichannel instruments such as the MRS-MIDI, GMR, and upgraded NUMIS Poly systems, which allowed data to be measured on multiple receivers simultaneously (Radic, 2006; Walsh, 2008; Girard et al., 2011). The MRS-MIDI is a low-current system designed for very shallow investigations down to approximately 10 m, whereas the GMR and NUMIS Poly systems are high-current systems (up to 800 A) designed for targets down to approximately 100 m. The multichannel capability sped up measurements in 2D/3D groundwater imaging (e.g., Walsh, 2008; Legchenko et al., 2011; Jiang et al., 2015) and allowed the use of remote reference noise-cancellation techniques. When the noise measured by a reference coil is highly correlated with the noise in the signal coil, a significant signal-to-noise ratio (S/N) improvement can often be achieved with reference noise cancellation (Walsh, 2008; Dalgaard et al., 2012; Müller-Petke and Costabel, 2014). Further changes included the use of untuned receiver coils (MRS-MIDI and GMR) and the digitization of raw measurements by a broadband circuit. Storing the raw measurements allowed for digital filtering and advanced signal-processing techniques such as powerline harmonics subtraction to be used, which often led to significant S/N enhancements (Larsen et al., 2014). By using tuned transmit circuitry and untuned receive circuitry, the instrument dead time was reduced to less than 3 ms with the GMR, improving the resolution of the early-time signal. However, the effective dead time of all surface NMR instruments is also associated with subsequent digital filtering in the signal-processing chain, which typically increases the dead time by a few ms (Dlugosch et al., 2011; Walsh et al., 2011). Development of surface NMR instruments has primarily been associated with commercial manufacturers. University research on instrumentation has been very scarce with the notable exception of the group at Jilin University in China (Lin et al., 2015).

Despite the achievements of existing surface NMR instruments, there are ample opportunities for further improvement. First, surface NMR measurements are known to be susceptible to noise and the S/N can be low at many sites. This makes investigations at many sites in developed areas infeasible, which has been a major obstacle preventing the widespread application of surface NMR. Second, the instrument dead time is limited by the switch operation from the transmit to the receive mode and the transient response of the analog filters. Third, phase information is not commonly used during inversion despite the fact that complex inversion has been demonstrated to improve imaging results (Braun et al., 2005; Behroozmand et al., 2012). This is in part because phase data are not available from all instruments and phase offsets induced by the instrument or signal-processing schemes can be difficult to determine and remove reliably (Irons and Li, 2014; Müller-Petke et al., 2016). Last but not least, surface NMR is a relatively time consuming and laborious geophysical measurement to acquire.

To address these shortcomings, we have developed a new compact surface NMR instrument called Apsu for hydrogeophysical investigations to a depth of 30 m. Apsu is designed as a compact, low-weight system with full control over pulses and pulse sequences. The instrument has a quasi-zero dead time, allows for the flexible deployment of small receiver coils attached to receiver units with wireless connections to a main unit, permits phase determination and calibration, and allows high measurement speeds. The Apsu system consists of a compact transmitter unit, a portable generator, an untuned transmitter coil, wireless GPS-synchronized receivers, and small untuned receiver coils. The untuned transmitter coil can remove the cumbersome tuning capacitor, and the instrument is powered by a small portable generator, which provides an alternative to the commonly used marine or car batteries.

This paper is organized as follows. A short introduction to surface NMR physics is followed by an overview of the new instrument and more detailed descriptions of the various subsystems. An example of field data is provided and is followed by discussions and a conclusion.

SURFACE NMR PHYSICS

To better understand the design choices behind the Apsu system, a brief description of surface NMR physics is first presented. Surface NMR uses an applied magnetic field $\mathbf{B_1}$ in the background of the earth's field $\mathbf{B_0}$ to produce measurable NMR signals from groundwater (e.g., Weichman et al., 2000; Hertrich, 2008). This is accomplished by transmitting an alternating current at or near the Larmor frequency f_L in a transmitter coil, where f_L is proportional to the local $\mathbf{B_0}$ and ranges from approximately 1 to 3 kHz worldwide. The perpendicular component of $\mathbf{B_1}$ relative to $\mathbf{B_0}$ perturbs the bulk hydrogen spin magnetization away from the longitudinal axis and toward the transverse plane. The pulse moment q is determined by the product of the transmitted current and the duration of the pulse. Stronger pulse moments increase the investigated volume in the subsurface and probe deeper than smaller pulse moments. In a full sounding, a range of pulse moments is used to illuminate the subsurface at different depths. Once the transmitting pulse is terminated, the transverse component of the bulk hydrogen spin magnetization precesses about the longitudinal axis at the Larmor frequency and relaxes back to equilibrium. The precessing magnetization generates an oscillating magnetic field that can be detected by a receiver coil as an induced voltage (Legchenko et al., 2002; Müller-Petke et al., 2016),

$$s(q,t) = s_0(q)e^{-t/T_2^*(q)}\cos(2\pi f_L t + \varphi(q)). \qquad (1)$$

The initial amplitude s_0 is proportional to the water content of the investigated volume, whereas the effective transverse relaxation time T_2^* may be empirically related to the pore size in the aquifer in the absence of magnetic geology (Grunewald and Knight, 2011). The relative phase $\varphi(q)$ is controlled by the subsurface conductivity, survey geometry, and pulse parameters (Trushkin et al., 1995).

THE APSU INSTRUMENT

This section provides an overview of choices made in the design of the Apsu instrument followed by an overview of the instrument and details of the various subsystems.

One of the motivations for the Apsu system development has been to obtain a highly flexible surface NMR system for research and production use. A large fraction of targets of interest is in the uppermost 30 m of the subsurface, and in these use cases, it is possible to trade the depth of investigation for the reduced size and weight of the instrument. Effectively, this means that a lower peak current system is opted for. With this choice, it is not necessary to use tuned transmitter coils; hence, the system does not use heavy, bulky tuning capacitors. One particular advantage of the small, lightweight instrument is the improved performance when conducting remote surveys, for example, in Arctic areas (Parsekian et al., 2013), on glaciers (Legchenko et al., 2011), or in otherwise difficult terrain (Irons et al., 2014; Keating et al., 2018). We opted to power the system from a lightweight generator. This ensures that power is available for long measurement runs or power-hungry pulse sequences without recharging or exchanging batteries.

A second, equally important, feature of driving an untuned transmitter coil is that amplitude and frequency modulation during the pulse are decoupled and arbitrary waveform pulse sequences can easily be produced with a pulse width modulation-based approach. This readily permits the use of complex pulses, for example, adiabatic pulses (Grunewald et al., 2016; Grombacher, 2017) and pulse sequences (Grunewald and Walsh, 2013). MRS-MIDI drives an untuned transmitter coil with low current, but it is not to our knowledge capable of implementing arbitrary pulse designs (Radic, 2006).

Surface NMR instrumentation has pushed toward short dead times to improve the S/N and detect fast-decaying NMR signals. With the Apsu instrument, we achieve short dead times by using separated transmitter and receiver coils. The separated coil approach avoids the dead time associated with active switching, for example, relays, at the expense of having to lay out additional receiver coils. However, the separation also improves resolution and permits the use of multiple receiver loops (Behroozmand et al., 2016).

The system has been designed in a modular fashion, and the transmitter and multichannel receiver system are independently operated. The system uses a Wi-Fi connection to transfer data and commands between a main unit and the transmitter/receiver unit. The receiver units are also used to record remote reference noise. In this case, the wireless connection ensures that the remote receiver coils can be placed independently from the transmitter system and can remain fixed when multiple soundings are carried out in an area.

Instrument overview

The instrument consists of a transmitter unit (ApsuTx), a power supply (ApsuPS), a generator, an untuned transmitter coil, a Wi-Fi antenna array mounted in a tower, and multiple receiver units (ApsuRx) connected to small receiver coils as shown in Figure 1. The transmitter and receivers are all controlled by a central unit (ApsuMaster) through the Wi-Fi link. Unobstructed, the Wi-Fi network has coverage of more than 1 km. The ApsuMaster is a compact field PC that runs the controller software and has independent TCP/IP sockets connecting it to each unit. The transmitter settings, for example, the pulse duration, current and frequency modulations, and receiver settings, for example, gain factors and synchronization time, are specified in the ApsuMaster and are transferred to each unit through the Wi-Fi connections. The use of a Wi-Fi network offers the ability to easily connect many receivers for 2D and 3D investigations and eliminate the cable layout to multiple receivers.

The lightweight (13 kg) generator outputs a 230 V alternating current (AC) that is delivered to the ApsuPS. To avoid electromagnetic noise from the generator coupling into the receiver coils, the generator is kept at a safe distance of more than 50 m away from the receiver coils. The power supply converts the AC to a controlled DC potential up to 600 V with a resolution of 1 V. Because the ApsuTx can draw an instantaneous current up to 150 kW, a more than 20 mF capacitor bank is used to maintain the excitation voltage during the pulses. This is especially important for multipulse scenarios such as Carr–Purcell–Meiboom–Gill sequence or T_1 measurements (Walbrecker et al., 2011; Grunewald and Walsh, 2013). The transmitter coil normally used is made from copper wire laid out in a 50×50 m coil geometry. The voltage and current ranges used in the Apsu instrument allow us to use thin, lightweight wire and the 6 kg transmitter coil is easily deployed. The low resistance of the transmitter coil dissipates little energy that reduces the recharge time between pulses. The excitation-current waveform is measured with a wide-bandwidth current probe (CP) directly attached to the transmitter coil and is used later for inversion.

The receiver system consists of independently operated data-acquisition boxes, each containing three channels (Liu et al., 2019a). Each channel can be connected to a differential coil with a low-noise preamplifier and a high-resolution acquisition board. The acquisition board contains multistage amplifiers, short settling-time filters, and two 24-bit analog-to-digital converters in dual-gain mode sampling at 31.25 kHz. For the standard 1D surface NMR survey, a central receiver coil measures the NMR signal and one or several ApsuRx boxes and receiver coils can be used to collect noise for remote reference noise cancellation. In 2D/3D groundwater imaging scenarios, multiple receiver coils and ApsuRx's may be placed inside the transmitter coil to measure signals at several places simultaneously. The ApsuRx collects data continuously and the segments containing NMR signal can be selected and retrieved by the ApsuMaster wirelessly. All transmit and receive units are synchronized to GPS, and the jitter between units is less than 100 ns.

Transmitter unit

In existing high-current surface NMR transmitters, external tuning capacitors are connected to the transmitter coil. This allows the resonance frequency to be adjusted to the local Larmor frequency and the excitation current to be maximized. These high-voltage tuning capacitors are large and relatively heavy. In contrast, Apsu uses an untuned transmitter coil, which removes the need for a tuning

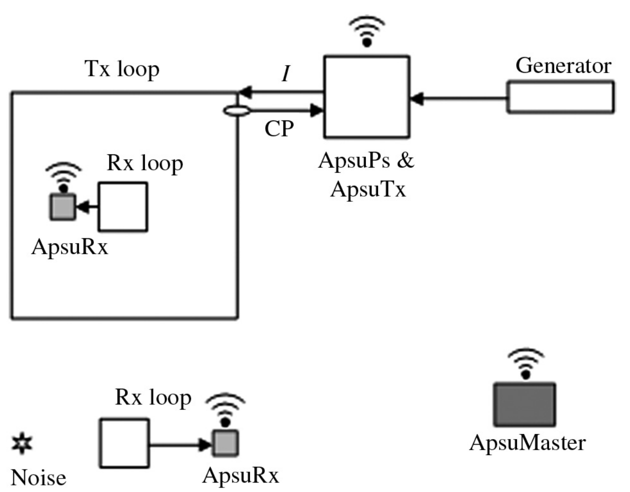

Figure 1. Diagram of the multichannel surface NMR system Apsu. The current in the transmitter coil I is monitored with a wide-bandwidth CP.

capacitor at the expense of a reduced maximum current. The transmitter current is ramped up and down linearly with a slope determined by the coil self-inductance and the transmitter voltage, resulting in an excitation pulse composed of independent triangles. The pulse frequency and current magnitude are modulated by designing the timing of the triangles allowing arbitrary pulses to be produced, including single-frequency pulses (such as on- or off-resonance pulses), pulses involving frequency sweeps such as adiabatic half passages (Grombacher et al., 2016b; Grunewald et al., 2016; Grombacher, 2017), and multipulse experiments (Grunewald and Walsh, 2013). The transmitter coil currently used is made from 3.3 mm^2 (AWG 12) standard stranded copper wire laid out in a 50×50 m coil geometry. It has a resistance of approximately 1 Ω and an inductance of approximately 0.54 mH. The coil is slightly overdamped, and the transmitter current decays to zero in a well-controlled manner after turn-off.

One oscillation of the triangular-shaped transmitter current waveform is schematically shown in Figure 2. The current starts ramping up from t_0 and continues until t_1 where the peak current is determined by

$$I = \frac{U}{L}\tau, \tag{2}$$

where U is the transmitter voltage, L is the inductance of the coil, and τ is the ramp-up time. The following half-cycle has alternative polarity and can be designed with independent τ. The timing between the triangles determines the pulse frequency. The transmitter coil inductance is measured by outputting a predesigned on-resonance pulse with a specific voltage U. The inductance is then computed from the slope of the measured ramp-up current. This measurement yields an accurate value for the inductance, which is used for the subsequent pulse design.

The instant transmitting frequency f of a triangle is given by $f = 1/2T$. For a given pulse moment, the ApsuPS voltage U is fixed and the peak current is determined by the ramp-up time τ, that is, a larger peak current is obtained by letting the current ramp-up for longer. The parameters $T(k)$ and $\tau(k)$ of the kth triangles can be designed independently. Varying $T(k)$ allows the frequency to be modulated during the pulse, whereas varying $\tau(k)$ allows the effective peak current to be modulated during the pulse. The parameters $T(k)$ and $\tau(k)$ are fixed for a specific surface NMR measurement, and different excitation pulse moments are obtained by adjusting U. In essence, the transmitter gives total control over the pulse sequence design by decoupling the amplitude and frequency modulations through pulse-width modulation.

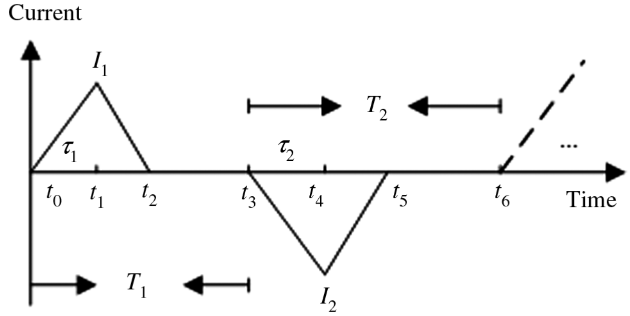

Figure 2. Schematic view of one oscillation in an Apsu excitation pulse. The half-cycle duration, peak current, and ramp-up time of the first triangle are T_1, I_1, and $\tau_1 = t_1 - t_0$, respectively.

In the Fourier domain, a triangle wave consists of a fundamental frequency component and higher order harmonics. However, only the energy content at the fundamental frequency can excite water because the higher order harmonics are too distant from the Larmor frequency to have an impact (Grombacher et al., 2016a). The effective current is written as

$$I_{f_L}(k) = \frac{4}{\pi^2}\frac{U}{L}\frac{1}{f(k)} \cdot \sin^2\left(\frac{\pi}{2}\alpha(k)\right), \tag{3}$$

where $\alpha(k) = \tau(k)/T(k)$ and $f(k)$ are the duty cycle and frequency for the kth triangle, respectively. A larger duty cycle has higher transmitting efficiency, which means that more energy is contained in the fundamental frequency component used to excite groundwater. For a constant duty cycle α, the effective current is only determined by the transmitter voltage U; therefore, increasing U can improve the transmitting current. The maximum effective current for a 50×50 m coil is 105 A when the Larmor frequency is 2150 Hz and α is 50%.

The energy stored in the capacitor bank transfers to the coil during current ramp-up, and most of the energy is recycled back to the bank during current ramp-down. Only a small amount of energy is dissipated in the coil resistance R. For an on-resonance pulse with duration τ_p, the energy loss is given by

$$\Delta E = \frac{R\tau_p}{6}\left(\frac{U}{Lf_L}\right)^2 \alpha^3. \tag{4}$$

The maximum energy loss ($\alpha = 50\%$, $U = 600$ V) for a $\tau_p = 50$ ms long on-resonance pulse with a 1 Ω Tx coil is 278 J. To resupply the energy lost during the excitation and prepare for the next pulse, the capacitor bank is recharged from the ApsuPS with a charging power of 600 W when $U = 600$ V, which means that at the highest output power, the transmitter is fully recharged in 0.5 s. At a lower output power, the recharging time is shorter. Hence, the transmitter is capable of generating large numbers of pulses in quick succession.

Figures 3, 4, and 5 present examples of the transmitter performance. The ability of the transmitter system to output repeatable pulses is demonstrated in Figure 3, where 120 subsequent, 52 ms single-frequency transmitter pulses with an effective current of 80 A are plotted on top of one another. The top panel shows the full waveform, and the bottom panel shows a magnification of a single oscillation. In both panels, the pulse-to-pulse variation is negligible; that is, the peak current in the positive half-oscillation in Figure 3b is 95.37 ± 0.05 A. A second important observation is that the current waveform is stable throughout the pulse and there is no decrease in the peak amplitude.

Figure 4 shows one oscillation from 20 pulses with peak currents ranging from 2.4 to 95 A, represented as light-gray to black lines, respectively. The stability of the waveform is maintained for all currents, and the peak current remains fixed in time for all pulses demonstrating the phase stability. An example of the ability of the transmitter system to output nonstandard waveforms is presented in Figure 5. The top panel shows the full waveform of an adiabatic pulse sweeping from 2250 to 2150 Hz in 50 ms. The two bottom panels magnify the early and late portions of the waveform where the frequency sweeping during the pulse is evident.

The system can also be used with coil sizes other than 50 × 50 m. Larger coils will have a higher self-inductance, and the peak current will therefore be reduced according to equation 2. If smaller coils with lower self-inductance are used, the system will be able to reach a maximum allowable current from the power supply, which is limited by the coil resistance, resulting in trapezoidal waveforms.

The ApsuPS is powered by a portable 1 kW motor generator. One important concern when using a generator is EM noise radiation. A field experiment studying the impact from generator noise was conducted by collecting noise with a roaming receiver coil at different offsets from the running generator, which was connected to a resistive load. The noise floor at each offset is compared to the background noise when the generator is switched off, and the result is shown in Figure 6. The measurement shows that the generator noise is negligible when the distance between the generator and the center of the receiver coil is more than 50 m.

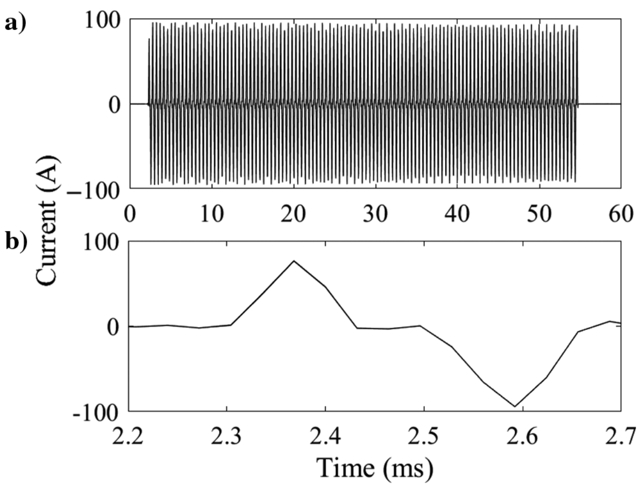

Figure 3. Repeatability of the transmitter pulses. In both figures, 120 subsequent pulses at an effective current of 80 A are plotted on top of one another: (a) Full pulse and (b) magnification on one oscillation.

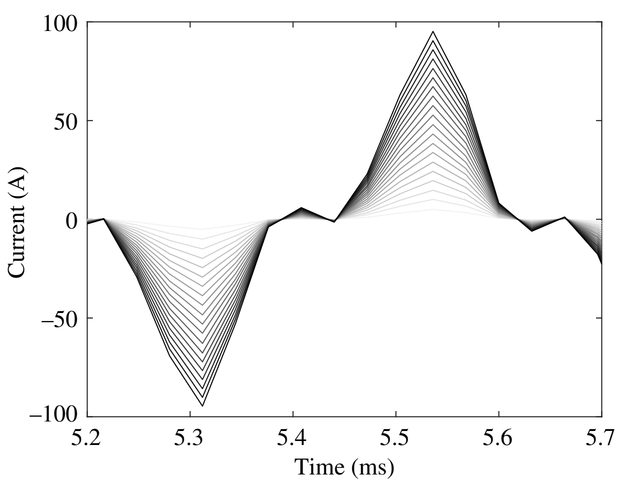

Figure 4. Stability of the transmitter pulses for different peak currents. The plot shows one oscillation from 20 pulses with peak currents between 2.4 (light gray) and 95 A (black). The transmitter pulses remain stable for all currents.

Multichannel wireless receiver system

A flexible multichannel receiver system has been developed for the Apsu instrument. Only a brief introduction to the receiver system is given here. Further details are available in Liu et al. (2019a). The Apsu system uses separate small receiver coils, which increases the setup time compared to a coincident coil setup, but it is also advantageous in several aspects. First, separated coils can reduce the instrument dead time by avoiding the switching operation in the coincident coil. Second, the central-coil configuration has been demonstrated to improve the investigation resolution (Behrooz-

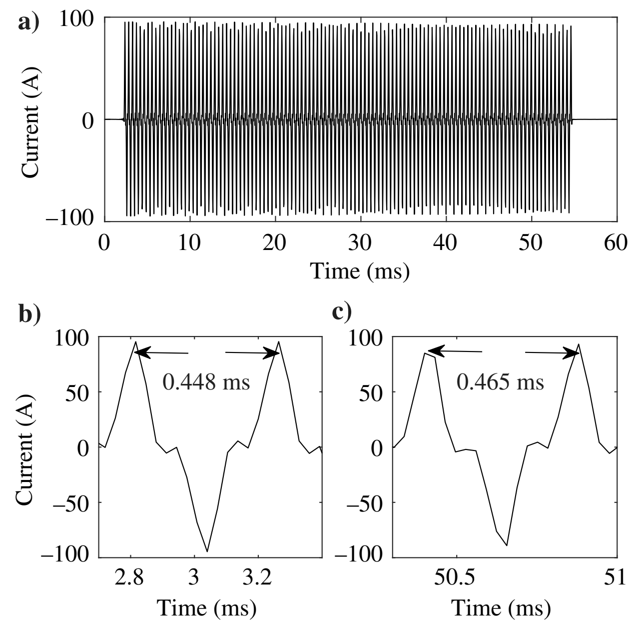

Figure 5. (a) Current waveform of an adiabatic pulse sweeping from 2250 to 2150 Hz in 50 ms. Magnified views of the start and the end of the pulse are shown in (b and c) separately. The arrows show the changing oscillation period throughout the adiabatic pulse.

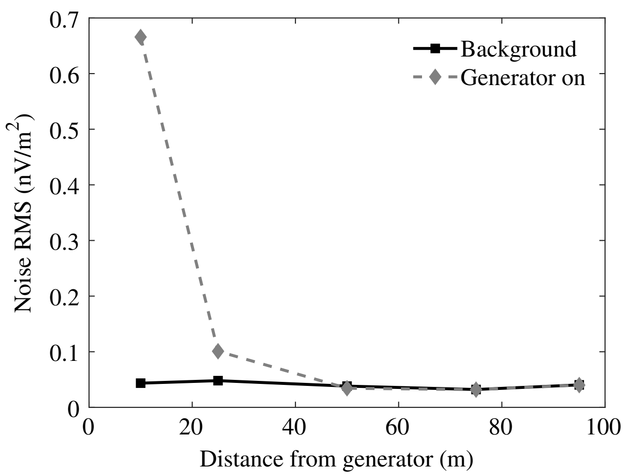

Figure 6. Noise floor with a running generator (the dashed gray line) compared to the background (the solid black line) at different distances between the receiver coil and generator.

mand et al., 2016). Third, the use of small coils leads to more rapid field deployment for multireceiver surveys, for example, for 2D/3D imaging (Jiang et al., 2015). Finally, wireless connections to remote reference noise coils are beneficial because these coils can remain stationary when several soundings are conducted in an area.

The minimum effective area of a receiver coil is recommended to be 500 m^2 to ensure satisfactory signal levels in low-water conditions (Grombacher et al., 2018). Larger effective areas cannot indefinitely improve S/N because the signal and the inductively coupled noise scale linearly with the effective area. A balance between satisfactory S/N and rapid deployment can be obtained by using small receiver coils.

We use 9×9 m, 12-turn differential coils with an effective area of 972 m^2 for signal and remote noise measurement. The untuned receiver coil has a cutoff frequency of 43 kHz, approximately 20 times higher than the local Larmor frequency. To reduce the influence of noise coupled into the transmission cables, a preamplifier is mounted directly at the receiver coil amplifying the signal before transmission to the receiver box. The preamplifier is an ultra-low-noise, low-distortion operational amplifier with a gain of 21 and a typical input noise voltage of 0.9 $\mathrm{nV}/\sqrt{\mathrm{Hz}}$ in the 1–3 kHz range.

The receiver coil and preamplifier are physically connected, meaning that the induced voltage can exceed the maximum input range of the preamplifier during the strong excitation pulses. To protect against overvoltage, a clamper shortens the input and clips the voltage to a safe range.

The acquisition board contains low-noise amplifiers, an analog low-pass filter, and a 24-bit high-resolution analog-to-digital converter (ADC). The low-pass filter has a cutoff frequency of 5 kHz with a corresponding settling time of 0.42 ms. A high-pass filter with a cutoff frequency of 1 kHz can be installed to remove low-frequency noise at the expense of 2 ms more settling time. Signals are continuously digitized with a sampling rate of 31.25 kHz and noise-only data are measured just before the transmit pulse are available for noise-reduction algorithms (Liu et al., 2018). Timing is controlled from GPS modules installed in all ApsuRx units and in the ApsuTx unit. The power consumption including the Wi-Fi antenna is approximately 12 W, and up to 8 hours of data collection can be performed on a single charge of a 9 Ah battery.

The ApsuRx can also work as an additional data logger using other transmitters, which has been demonstrated with the NUMIS Poly instrument in Grombacher et al. (2018) and the GMR instrument in Liu et al. (2019a). A photograph of all the Apsu system components is shown in Figure 7.

Figure 7. The Apsu system. (1) ApsuPS, (2) generator, (3) ApsuTx, (4–6) ApsuRx, and (7) transmitter and receiver coils. The photo also shows the communication and power cables.

Instrument dead time

To quantify the instrument dead time, a measurement was conducted with the 9×9 m, 12-turn receiver coil placed in the center of the 50×50 m transmitter coil. The transmitted frequency was 2150 Hz, and the peak current was approximately 50 A. An example of synchronous measurements of the transmitter current and receiver voltage is shown in Figure 8.

In Figure 8a and 8b, the pulse is observed by the CP and the receiver coil, respectively. Figure 8c and 8d shows a magnification of the start and end parts of the pulse, respectively. The transmitter current (the red line) is shown as triangles, and the receiver voltage (the blue line) is clamped when the observed signal from the transmitter exceeds approximately 60 μV. The receiver coil voltage drops to the normal noise floor after the pulse is terminated. It is seen that the receiver voltage is synchronous with the transmitter starting to rise at 2.24 ms where the transmitter current starts ramping up. In Figure 8d, the transmitter current is terminated at 54.75 ms. In the untuned transmitter coil, the last triangle ramps down to zero and there are no oscillations after the pulse is terminated. However, due to the low-pass filter in the signal chain, the receiver voltage requires additional time to reach the noise floor. Additionally, the capacitors in the low-pass filter are charged during excitation and start to discharge after the pulse is terminated. The discharge waveform is seen by the receiver coil as an exponentially decaying curve (the dashed black line) with the beginning clipped as can be seen from the last trapezoid of the receiver voltage shown in Figure 8d. The dead time of the system is reduced by fitting a monoexponential model to the decay and subtracting the model from the measured data. In practice, this improves the dead time by approximately 2 ms. After subtraction, the receiver voltage reaches the noise floor at 55.52 ms. The difference between this time stamp and the transmitter current being terminated at 54.75 ms is the instrument dead time, which is 0.77 ms. The instrument dead time is mainly limited by the saturation of the analog low-pass filter.

In the subsequent signal-processing chain, the spectral-analysis method is applied (Liu et al., 2019b). This implies that no further digital filters are involved; hence, 0.77 ms is the effective dead time of the Apsu system.

Phase determination

Besides the initial amplitude and relaxation rate, a surface NMR signal is also characterized by its phase relative to the transmit pulse. It has been shown that complex inversion incorporating phase information can improve the investigation depth and resolution (Braun et al., 2005; Irons and Li, 2014). The phase of the NMR signal arises due to the polarization change induced by the propagation of the excitation field through a conductive medium (Trushkin et al., 1995; Weichman et al., 2000; Lehmann-Horn et al., 2012), survey geometry (Behroozmand et al., 2016), and pulse parameters (Grombacher et al., 2016b). Although the mechanisms responsible for determining the signal phase are included in forward modeling, some studies are confronted with a constant phase shift in the collected data (Irons and Li, 2014; Roy and Lubczynski, 2014). Potential reasons for the constant phase shifts include instrumentation and signal-processing effects.

The instrument sources of the phase shift include the synchronization lag between the transmitter and receiver, the phase response of the CP, receiver coils, and the acquisition circuit itself. In Apsu, the jitter between the transmitter and receiver is determined by the GPS clock. The jitter is less than 100 ns and is negligible in phase considerations. The phase of the transmitting signal φ_T is computed by a least-squares fitting of the last several half-cycles of the excitation-current waveform with a sinusoidal oscillation at the transmit frequency f_T. Subsequently, φ_T is extrapolated to the beginning of the extracted envelope, which is the start time t_s of the first sliding window. An example of the extracted phase from the excitation current, extrapolated to the beginning of the signal envelope, is illustrated in Figure 9. The example uses a 52.51 ms adiabatic pulse.

The transmitter current waveform shown in Figure 9a is used to estimate the accurate excitation current and transmit phase. The fitting of the current time series starts at 51.58 ms, which defines the origin of time, and it ends at 54.75 ms. The magnitude of the fitted sinusoidal waveform is smaller than the peak transmitter current of the triangle, and the ratio between them is determined by the duty cycle α.

In Figure 9b, the envelope extracted using the spectral-analysis method starts at 55.52 ms. The fitted phases are 76.6° and 0.6° for the transmitter current and NMR signal φ_R, respectively. When the same fitting procedure is applied to the measured current waveform of other pulse moments with identical pulse shapes but different peak currents, the phase deviation between different moments is found to be less than 1° between different peak currents, implying a consistent transmit phase retrieval.

The contributions to the phase between transmitted and received signals from the instrument and coil geometry can be determined directly. We do this by transmitting a very low-current NMR pulse and directly measuring the transmitted signal in the receiver coil using the lowest gain settings in the programmable gain amplifiers.

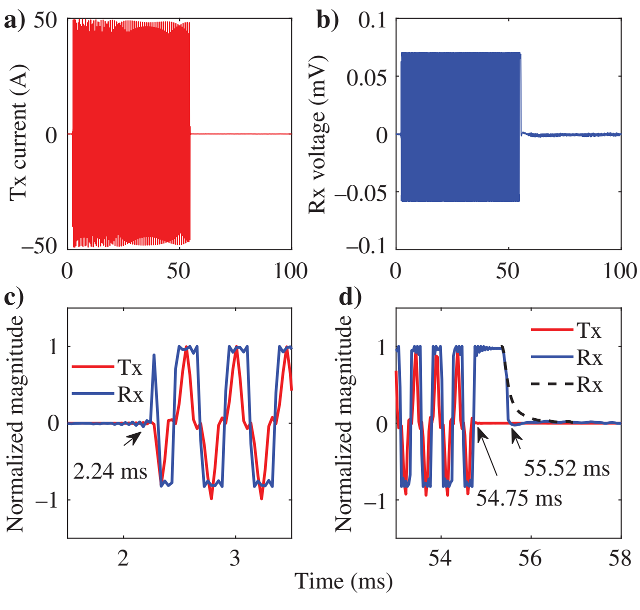

Figure 8. Measurements of the (a) transmitter current and (b) receiver signal with a 50 A, 52.51 ms adiabatic pulse. The current is measured by the transmitter using a CP, and the receiver voltage is recorded by an ApsuRx using a 9×9 m, 12-turn coil. (c and d) Magnified plots of the start and end parts of the transmitter current (red) and receiver voltage (blue). The magnitudes in (c and d) are normalized to compare the timing. The dashed black line in (d) shows the receiver voltage before subtraction of the exponential decay of the capacitor discharging voltage.

The low-current and amplifier gain setting is used to avoid saturation in the receiver system, and it also ensures that no NMR signal from water can distort the measurement. A small segment from such a measurement is given in Figure 10, based on a 40 ms pulse, a transmitter current of 0.13 A, and a frequency of 2147 Hz. The red and blue dots show the normalized transmitter current and receiver voltages, respectively, and the solid lines show sinusoidal fits at the transmitted Larmor frequency. The difference between the two phase of two signals is $-25.0° \pm 2.3°$. The reason that the receiver signal leads the transmitter signal is ascribed to an additional delay in the signal chain caused by the CP. Importantly, this measurement allows for a calibration of the instrument and coil geometry phase; that is, the remaining phase in the measured data is solely caused by the earth response.

FIELD RESULTS

Field measurements were conducted in the Kompedal forest near Silkeborg, Denmark, to demonstrate the performance of the Apsu system. This site has low artificial noise and is suitable for system verification. Prior information from previous ground-based transient electromagnetics (TEM) measurements indicates a thick resistive unit extending to a depth of 30 m, underlain by a more resistive unit. The site has previously been used to investigate the feasibility of small receiver coils with the NUMIS Poly system (Grombacher et al., 2018). In the previous measurements, a NUMIS Poly was used as the surface NMR transmitter and the NMR signals were measured with the Apsu receiver system. In the measurements presented here, only the Apsu system is used.

A 50×50 m, single-turn transmitter coil and a 9×9 m, 12-turn receiver coil are placed in the central-coil configuration. The induct-

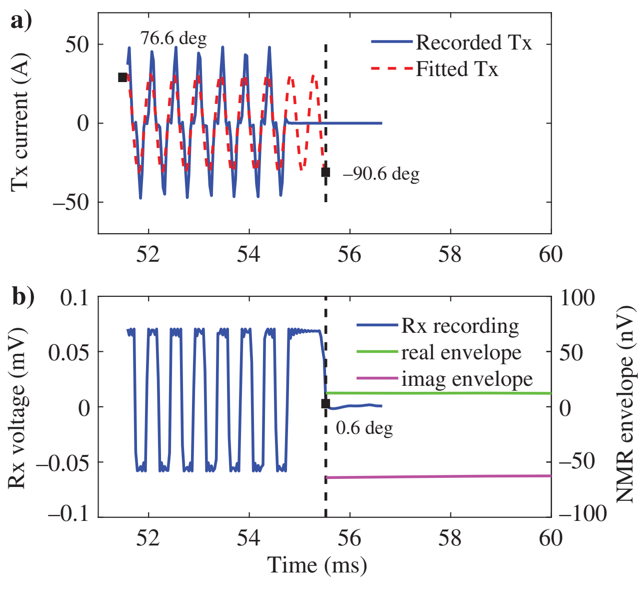

Figure 9. (a) Phase fitted to the transmitter current and (b) the extracted envelope of the NMR signal. Note that only the end part of the pulse is shown and the beginning of the receiver signal (blue line) is truncated during excitation. The dashed red curve in (a) shows the extrapolated current waveform toward the NMR signal part ending at the dead time indicated by the vertical dashed black lines. The real and imaginary envelopes are given by the green and magenta lines in (b), respectively.

ance of the transmitter coil was measured to be 0.54 mH. The Larmor frequency was measured to be approximately 2150 Hz at the site. Nine measurements were conducted in four hours with different

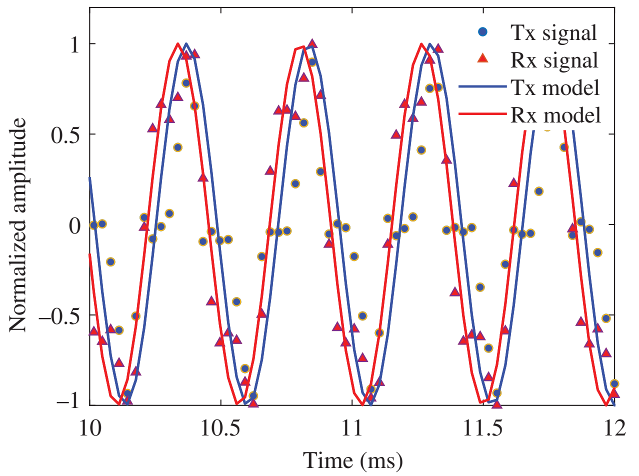

Figure 10. Measurement of the phase difference between the transmitter and receiver signals stemming from instrument factors and coil geometry only. The dots show measured data, and the full lines show sinusoidal fits at the Larmor frequency of 2147 Hz.

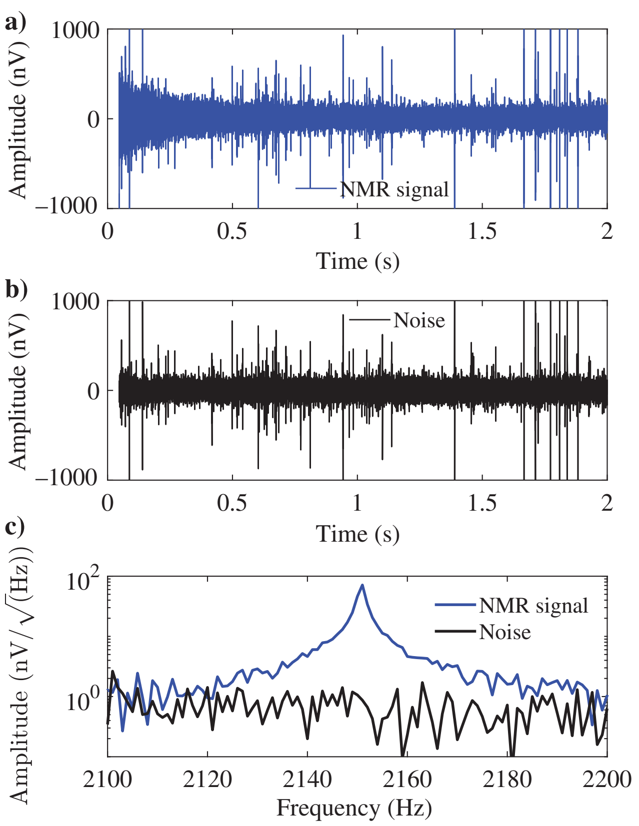

Figure 11. Time series of (a) stacked measurements and (b) noise obtained with a transmitter current of 50 A. (c) Spectrum of the NMR signal and noise; the blue curve is the NMR signal, and the black curve is the noise floor. Note that the spectral amplitude is plotted on a logarithmic scale.

excitation pulses: one on-resonance pulse, two off-resonance pulses with $\Delta f = \pm 3$ Hz, and six numerically optimized modulation (NOM) adiabatic pulses sweeping bidirectionally from 100 Hz offset and terminating at 2148, 2150, and 2153 Hz.

In the on-resonance measurement with a 40.5 ms pulse, 20 linearly spaced currents between 4 and 90 A were generated, corresponding to pulse moments between 0.16 and 3.6 A. For each current level, 16 stacks were acquired. The stacked measurements and the corresponding spectrum for a transmitter current of 50 A are shown in Figure 11.

After stacking, the NMR signal (blue) with decaying amplitude is clearly visible with an initial amplitude of 280 nV (Figure 11a). The noise data (black) are obtained by stacking the measurements with alternating polarity to cancel the NMR signal. The noise consists of instrument noise, spikes, powerline harmonics, and external random noise. The rms value of the noise, measured on segments without spikes, is approximately 98 nV. Three spikes can be observed in the NMR signal and noise data at the synchronous segments. All of the observed spikes have a duration shorter than 0.5 ms, which is consistent with impulsive noise excitation of the Apsu low-pass filter with its associated settling time of 0.42 ms.

The amplitudes of the powerline harmonics with orders higher than 20 are relatively low at this site, and no powerlines are visible in the amplitude spectrum of stacked data shown in Figure 11c. As seen in the spectrum, the NMR signal component has a peak amplitude of 70 nV/$\sqrt{\text{Hz}}$, whereas the noise floor is approximately 1 nV/$\sqrt{\text{Hz}}$. The complex envelopes extracted using the spectral-analysis method (Liu et al., 2019b) in the on-resonance pulse measurement are shown for all of the pulse moments in Figure 12.

Two examples of the envelopes measured with the 2150 Hz on-resonance pulse and transmitting currents of 4 and 90 A, corresponding to the smallest and largest used pulse moments, are shown in Figure 13. Even for these pulse moments in which the NMR signal is low (Figure 12) we still observe high-S/N envelopes.

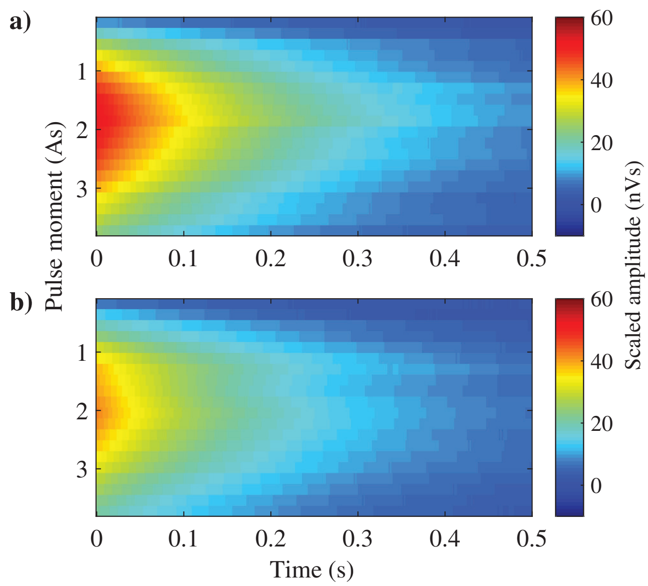

Figure 12. (a) Real and (b) imaginary components of the NMR envelopes of an on-resonance pulse measurement extracted using spectral analysis.

An example of the results obtained with a 55.52 ms NOM adiabatic pulse sweeping from 2250 to 2150 Hz is given in Figure 14. Similar to the above results, high-S/N data are obtained for all pulse moments.

DISCUSSION

One of the goals in the development of the Apsu system has been to provide a highly flexible surface NMR system for research and production use. As an example, the system has the potential to decrease the measurement time of 2D/3D groundwater investigations in which the use of small, wirelessly connected receiver coils can significantly speed up field deployment.

The Apsu system features a smaller peak current than some commercial instruments, which translates to the shallower depth of investigation. However, most of our current hydrogeologic research targets are in the top 20–30 m of the subsurface and an analysis based on the approach discussed by Müller-Petke and Yaramanci (2008) shows the depth of investigation to be approximately 30 m for a 65 ms pulse given the loop geometries and current amplitudes typical for an Apsu survey. The depth of investigation can be increased through the use of longer pulses giving large pulse moments, but this requires a trade-off between the penetration depth and sensitivity to fast decaying signals because relaxation during pulse effects becomes more pronounced for longer pulse lengths.

If deeper targets are to be imaged, the peak current must be increased. In an untuned transmitter coil, the maximum current for a given frequency is limited by the transmitter voltage and the transmitter coil's self-inductance as expressed in equation 2. To increase the transmitter current, the voltage U needs to be increased, which would warrant additional electronic development and safety engineering. However, another approach made possible by the compactness and design of the Apsu system is to drive two transmitter coils simultaneously using two synchronized transmitters. Such an approach can potentially double the peak current assuming negligible coupling between coils, and it opens up the possibility of exploring advanced transmit pulse and pulse sequence scenarios.

The wireless connection between the ApsuMaster unit and the ApsuRx units and receiver coils makes it possible to locate remote receiver coils further away from the surface NMR instrument than normally, and the receiver coils can be placed in the vicinity of identified noise sources.

As shown above, the phase of the NMR response relative to the transmit pulse can be reliably retrieved with the Apsu system. Ongoing work is devoted to fully model, measure, and account for all instrumental contributions to this phase. When these contributions are removed from measured NMR data, the remaining phase is controlled by the subsurface conductivity, transmit and receiver coil geometry, and transmit frequency. These parameters can all be independently measured, that is, subsurface conductivity can be obtained from a TEM sounding, or they can be computed and included in NMR forward models. This implies that the phase can be used to constrain complex inversions, rather than being a free parameter that must be solved for in the inversion. Effectively, this will reduce modeling errors and improve the resolution of surface NMR.

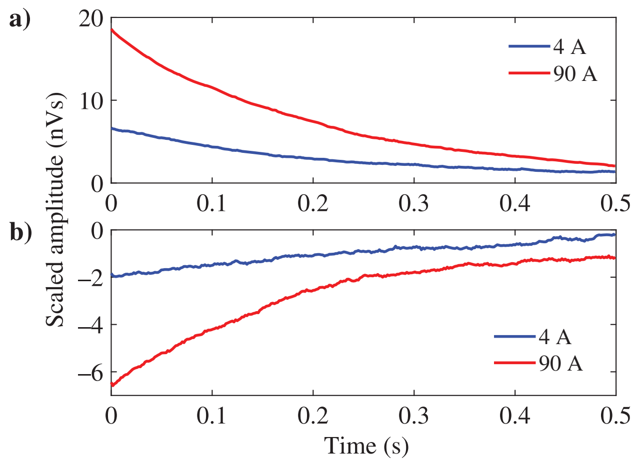

Figure 13. (a) Real and (b) imaginary components of the NMR envelopes for the on-resonance pulse using transmitting current 4 (blue) and 90 A (red).

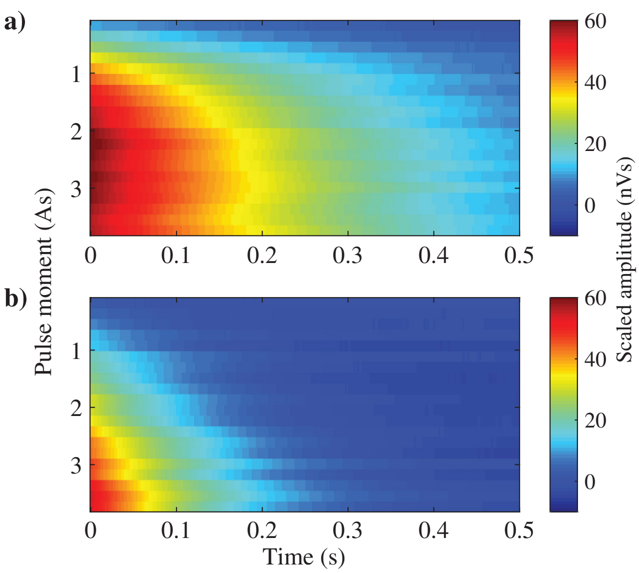

Figure 14. (a) Real and (b) imaginary components of the NMR envelopes extracted using spectral analysis. The transmit scheme is an adiabatic NOM pulse sweeping from 2250 to 2150 Hz in 55.52 ms.

CONCLUSION

We have presented a new surface NMR system, Apsu, developed for fast and efficient subsurface imaging. The system is based on a compact transmitter, powered from a lightweight portable generator. The transmitter drives an untuned coil, and tuning capacitors are not included in the design, reducing weight with the trade-off of peak current. The transmitter current waveform is triangular with a maximum effective current of 105 A. Each triangle in the waveform can be independently modulated; hence, the system offers great freedom in the design of NMR pulses and pulse sequences. In standard operation, an NMR pulse is transmitted every 3 s, implying that a 20 pulse moments, 30 stack survey can be completed in half an hour. The receiver system is physically separated from the transmitter system. Instead, the NMR signal is measured inductively by one or more small receiver coils connected to receiver boxes. Each receiver box is synchronized by GPS and is wirelessly connected to a master unit for increased flexibility in fieldwork.

Using field data acquired in Denmark, we have demonstrated that the Apsu system is capable of high-S/N imaging of subsurface groundwater using on-resonance and adiabatic pulses with subms dead times. The Apsu system is now in regular use for hydrogeologic studies, and it further provides a flexible platform for future research in surface NMR instrumentation, signal processing, pulse design, modeling, and inversion.

ACKNOWLEDGMENTS

S. Ejlertsen, S. M. Dath, and C. Nedergaard are gratefully acknowledged for their efforts in building the system. The work was supported by grants from the Chinese Scholarship Council, the Independent Research Fund Denmark, the COWI Foundation, and the Aarhus University Research Foundation.

DATA AND MATERIALS AVAILABILITY

Data associated with this research are available and can be obtained by contacting the corresponding author.

REFERENCES

Behroozmand, A. A., E. Auken, G. Fiandaca, A. V. Christiansen, and N. B. Christensen, 2012, Efficient full decay inversion of MRS data with a stretched-exponential approximation of the T_2^* distribution: Geophysical Journal International, **190**, 900–912, doi: 10.1111/j.1365-246X.2012.05558.x.

Behroozmand, A. A., E. Auken, G. Fiandaca, and S. Rejkjaer, 2016, Increasing the resolution and the signal-to-noise ratio of magnetic resonance sounding data using a central loop configuration: Geophysical Journal International, **205**, 243–256, doi: 10.1093/gji/ggw004.

Behroozmand, A. A., K. Keating, and E. Auken, 2015, A review of the principles and applications of the NMR technique for near-surface characterization: Surveys in Geophysics, **36**, 27–85, doi: 10.1007/s10712-014-9304-0.

Bernard, J., 2007, Instruments and field work to measure a magnetic resonance sounding: Boletín Geológico y Minero, **118**, 459–472.

Braun, M., M. Hertrich, and U. Yaramanci, 2005, Study on complex inversion of magnetic resonance sounding signals: Near Surface Geophysics, **3**, 155–163, doi: 10.3997/1873-0604.2005011.

Dalgaard, E., E. Auken, and J. J. Larsen, 2012, Adaptive noise cancelling of multichannel magnetic resonance sounding signals: Geophysical Journal International, **191**, 88–100, doi: 10.1111/j.1365-246X.2012.05618.x.

Dlugosch, R., M. Müller-Petke, T. Günther, S. Costabel, and U. Yaramanci, 2011, Assessment of the potential of a new generation of surface nuclear magnetic resonance instruments: Near Surface Geophysics, **9**, 89–102, doi: 10.3997/1873-0604.2010063.

Girard, J.-F., J. Bernard, and B. Texier, 2011, Application of remote filtering to magnetic resonance sounding using multi-channel data acquisition: Symposium on the Application of Geophysics to Engineering and Environmental Problems, 75, doi: 10.4133/1.3614232.

Grombacher, D., 2017, Numerically optimized modulations for adiabatic pulses in surface nuclear magnetic resonance: Geophysics, **83**, no. 2, JM1–JM14, doi: 10.1190/geo2016-0574.1.

Grombacher, D., J. J. Larsen, and E. Auken, 2016a, Potential for square wave transmitters in surface NMR: Near Surface Geoscience 2016 — 22nd European Meeting of Environmental and Engineering Geophysics, doi: 10.3997/2214-4609.201602008.

Grombacher, D., L. Liu, J. J. Larsen, and E. Auken, 2018, Practical considerations for small receive coils in surface NMR: Journal of Applied Geophysics, **154**, 81–92, doi: 10.1016/j.jappgeo.2018.04.005.

Grombacher, D., M. Müller-Petke, and R. Knight, 2016b, Frequency cycling for compensation of undesired off-resonance effects in surface nuclear magnetic resonance: Geophysics, **81**, no. 4, WB33–WB48, doi: 10.1190/geo2015-0181.1.

Grunewald, E., D. Grombacher, and D. Walsh, 2016, Adiabatic pulses enhance surface nuclear magnetic resonance measurement and survey speed for groundwater investigations: Geophysics, **81**, no. 4, WB85–WB96, doi: 10.1190/geo2015-0527.1.

Grunewald, E., and R. Knight, 2011, The effect of pore size and magnetic susceptibility on the surface NMR relaxation parameter T_2^*: Near Surface Geophysics, **9**, 169–178, doi: 10.3997/1873-0604.2010062.

Grunewald, E., and D. Walsh, 2013, Multiecho scheme advances surface NMR for aquifer characterization: Geophysical Research Letters, **40**, 6346–6350, doi: 10.1002/2013GL057607.

Hertrich, M., 2008, Imaging of groundwater with nuclear magnetic resonance: Progress in Nuclear Magnetic Resonance Spectroscopy, **53**, 227–248, doi: 10.1016/j.pnmrs.2008.01.002.

Irons, T., and Y. Li, 2014, Pulse and Fourier transform surface nuclear magnetic resonance: Comprehensive modelling and inversion incorporating complex data and static dephasing dynamics: Geophysical Journal International, **199**, 1372–1394, doi: 10.1093/gji/ggu323.

Irons, T. P., K. E. Martin, C. A. Finn, B. R. Bloss, and R. J. Horton, 2014, Using nuclear magnetic resonance and transient electromagnetics to characterise water distribution beneath an ice covered volcanic crater: The case of Sherman Crater Mt. Baker, Washington: Near Surface Geophysics, **12**, 285–296, doi: 10.3997/1873-0604.2014009.

Jiang, C., M. Müller-Petke, J. Lin, and U. Yaramanci, 2015, Magnetic resonance tomography using elongated transmitter and in-loop receiver arrays for time-efficient 2-D imaging of subsurface aquifer structures: Geophysical Journal International, **200**, 824–836, doi: 10.1093/gji/ggu434.

Keating, K., A. Binley, V. Bense, R. L. V. Dam, and H. H. Christiansen, 2018, Combined geophysical measurements provide evidence for unfrozen water in permafrost in the Adventdalen valley in Svalbard: Geophysical Research Letters, **45**, 7606–7614, doi: 10.1029/2017GL076508.

Larsen, J. J., E. Dalgaard, and E. Auken, 2014, Noise cancelling of MRS signals combining model-based removal of powerline harmonics and multichannel Wiener filtering: Geophysical Journal International, **196**, 828–836, doi: 10.1093/gji/ggt422.

Legchenko, A., J.-M. Baltassat, A. Beauce, and J. Bernard, 2002, Nuclear magnetic resonance as a geophysical tool for hydrogeologists: Journal of Applied Geophysics, **50**, 21–46, doi: 10.1016/S0926-9851(02)00128-3.

Legchenko, A., M. Descloitres, C. Vincent, H. Guyard, S. Garambois, K. Chalikakis, and M. Ezersky, 2011, Three-dimensional magnetic resonance imaging for groundwater: New Journal of Physics, **13**, 025022, doi: 10.1088/1367-2630/13/2/025022.

Lehmann-Horn, J. A., M. Hertrich, S. A. Greenhalgh, and A. G. Green, 2012, On the sensitivity of surface NMR in the presence of electrical conductivity anomalies: Geophysical Journal International, **189**, 331–342, doi: 10.1111/j.1365-246X.2012.05380.x.

Lin, T., W. Chen, W. Du, and J. Zhao, 2015, Signal acquisition module design for multichannel surface magnetic resonance sounding system: Review of Scientific Instruments, **86**, 114702, doi: 10.1063/1.4934969.

Liu, L., D. Grombacher, E. Auken, and J. J. Larsen, 2018, Removal of co-frequency powerline harmonics from multichannel surface NMR data: IEEE Geoscience and Remote Sensing Letters, **15**, 53–57, doi: 10.1109/LGRS.2017.2772790.

Liu, L., D. Grombacher, E. Auken, and J. J. Larsen, 2019a, Apsu: A wireless multichannel receiver system for surface-NMR groundwater investigations: Geoscientific Instrumentation, Methods and Data Systems, **8**, 1–11, doi: 10.5194/gi-8-1-2019.

Liu, L., D. Grombacher, E. Auken, and J. J. Larsen, 2019b, Complex envelope retrieval for surface nuclear magnetic resonance data using spectral analysis: Geophysical Journal International, **217**, 894–905, doi: 10.1093/gji/ggz068.

Müller-Petke, M., M. Braun, M. Hertrich, S. Costabel, and J. Walbrecker, 2016, MRSmatlab — A software tool for processing, modeling, and inversion of magnetic resonance sounding data: Geophysics, **81**, no. 4, WB9–WB21, doi: 10.1190/geo2015-0461.1.

Müller-Petke, M., and S. Costabel, 2014, Comparison and optimal parameter settings of reference based harmonic noise cancellation in time and frequency domains for surface-NMR: Near Surface Geophysics, **12**, 199–210, doi: 10.3997/1873-0604.2013033.

Müller-Petke, M., and U. Yaramanci, 2008, Resolution studies for magnetic resonance sounding (MRS) using the singular value decomposition: Journal of Applied Geophysics, **66**, 165–175, doi: 10.1016/j.jappgeo.2007.11.004.

Parsekian, A. D., G. Grosse, J. O. Walbrecker, M. Müller-Petke, K. Keating, L. Liu, B. M. Jones, and R. Knight, 2013, Detecting unfrozen sediments below thermokarst lakes with surface nuclear magnetic resonance: Geophysical Research Letters, **40**, 535–540, doi: 10.1002/grl.50137.

Radic, T., 2006, Improving the signal-to-noise ratio of surface NMR data due to the remote reference technique: Near Surface 2006 — 12th EAGE European Meeting of Environmental and Engineering Geophysics, doi: 10.3997/2214-4609.201402690.

Roy, J., and M. Lubczynski, 2003, The magnetic resonance sounding technique and its use for groundwater investigations: Hydrogeology Journal, **11**, 455–465, doi: 10.1007/s10040-003-0254-8.

Roy, J., and M. W. Lubczynski, 2014, Exploiting the MRS-phase information to enhance detection of masked deep aquifers: Examples from the Netherlands: Near Surface Geophysics, **12**, 309–324, doi: 10.3997/1873-0604.2013058.

Schirov, M., A. Legchenko, and G. Creer, 1991, A new direct non-invasive groundwater detection technology for Australia: Exploration Geophysics, **22**, 333–338, doi: 10.1071/EG991333.

Trushkin, D. V., O. A. Shushakov, and A. V. Legchenko, 1995, Surface NMR applied to an electroconductive medium: Geophysical Prospecting, **43**, 623–633, doi: 10.1111/j.1365-2478.1995.tb00271.x.
Walbrecker, J. O., M. Hertrich, J. A. Lehmann-Horn, and G. G. Alan, 2011, Estimating the longitudinal relaxation time T1 in surface NMR: Geophysics, **76**, no. 2, F111–F122, doi: 10.1190/1.3549642.
Walsh, D. O., 2008, Multi-channel surface NMR instrumentation and software for 1D/2D groundwater investigations: Journal of Applied Geophysics, **66**, 140–150, doi: 10.1016/j.jappgeo.2008.03.006.
Walsh, D. O., E. Grunewald, T. Peter, H. Andrew, and F. Paul, 2011, Practical limitations and applications of short dead time surface NMR: Near Surface Geophysics, **9**, 103–113, doi: 10.3997/1873-0604.2010073.
Weichman, P. B., E. M. Lavely, and M. H. Ritzwoller, 2000, Theory of surface nuclear magnetic resonance with applications to geophysical imaging problems: Physical Review E, **62**, 1290–1312, doi: 10.1103/PhysRevE.62.1290.